Contrast agent separation in spectral micro CT with Medipix3 detector

JC Rodriguez Luna¹, Ian Harmon¹, and Mini Das^{1,2,*}

Department of Physics, University of Houston, Houston 77204, USA
 Department of Biomedical Engineering, University of Houston, Houston 77204, USA

ABSTRACT

X-ray image classification of anatomical structures or tissue types is critical for diagnosing lesions of various kinds. Differentiation of different contrast agents and bone is essential for such accurate classification in a range of applications. The complex tissue composition in organs presents a challenge for many material decomposition methods, which assume a limited number (two or three) of materials in the mixture. However, spectral information in x-ray imaging allows for improved material differentiation. In recent years, multi-energy computed tomography (CT) is becoming possible thanks to photon-counting detectors (PCDs). PCDs allow sorting incoming x-ray photons to discrete energy bins. These technological advancements represent promising opportunities for material decomposition. This paper first introduces a spectral distortion correction based on a per-pixel calibration and subsequently a material decomposition method that takes full advantage of the spectral information that PCDs provide. We show our results using Medipix3 class of PCDs. In our approach, we solve the decomposition problem through a series of steps, each time using cluster analysis to separate one new material from the multi-material object. The experimental results show that our spectral correction and high-dimensional data clustering reduces noise and improve decomposition accuracy.

Keywords: Material decomposition, Spectral CT, Contrast agents, Bone discrimination, Photon-counting detector, Medipix

1. INTRODUCTION

In conventional CT, only the cumulative attenuation contribution of the composite materials is measured, not the individual contribution of each component. This leads to a lack of specificity in separating contrast agents from bone or alcifications.^{1,2} Contrast agents with high atomic numbers (Z) are differentiable due to the characteristic K-edge energies. However, there are still challenges when the task involves separating multiple tissue types and contrast agents simultaneously.

The spectral capabilities of Medipix3 photon-counting detectors(PCDs) represent a promising opportunity for material decomposition and quantitative CT in general. For example, PCDs allow imaging and decomposing a wide selection of contrast agents.^{3–5} Even though PCDs have many advantages, they are not perfect; they show spectral distortions due to physical effects in the detector such as charge sharing, K-escape energy loss, pulse pileup and inter-pixel variability.^{6,7} Crystal defects that originate during the fabrication process usually change the individual pixel's response, generating noise and ring artifacts during the CT reconstruction. As a result, spectral distortion corrections are fundamental to improving material decomposition performance. In this paper, to address spectral distortions, we first remove the inter-pixel variability using a signal to equivalent PMMA thickness calibration approach similar to the one proposed by Jackubeck et al.,⁸ which we have repurposed to CT applications. Subsequently, we associate the corrected intensities to a set of ideal PMMA mass attenuation values. One of the main advantages of this approach is its simplicity and versatility, as it does not require the formulation of the detector's response model.

PCDs show the most promise in material decomposition applications, specifically in applications that use materials with K-edge in the diagnostic energy range (30-100keV). PCDs generate valuable spectral information in this range, but we need to incorporate cluster analysis in the material decomposition process to take full advantage of spectral data. The classical approach of single-step (dual-energy) material decomposition is no longer acceptable because it only uses a fraction of the available information. For example, prior work by Le and Molloi found that direct material decomposition of closely related materials from multi-energy data is generally unsuccessful.^{9,10}

Several multi-material decomposition methods have been proposed to bypass the two-material limitation of dualenergy CT and increase the total number of materials that can be discriminated and quantified. These methods use spectral information to reduce the number of estimated materials. However, most of these approaches are threshold-based image segmentation techniques^{2,11,12} which require a user-defined threshold for the segmentation. One of the main benefits of our method comes from our approach to material basis reduction, which utilizes all the available spectral information and achieves multi-material decomposition without the need for any user-defined thresholding. We demonstrate the simultaneous decomposition of several materials, including two contrast agents, using a CdTe-1mm Medipix detector to validate our technique. This study also explores the benefit of our spectral correction and unsupervised clustering on mass attenuation and mass fraction accuracy.

2. MATERIAL AND METHODS

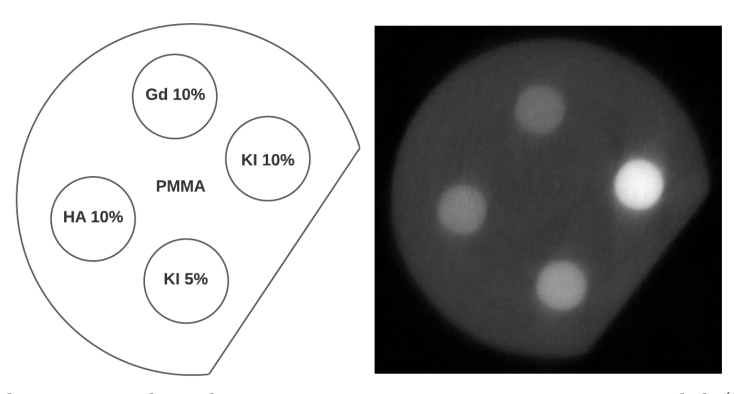


Figure 1: The PMMA phantom used in these experiments contains potassium iodide(KI) 10% water solution, potassium iodide(KI) 5% water solution, Gadopentetic acid($C_{14}H_{20}GdN_3O_{10}-H_2O$) 10% water solution, and hydroxyapatite($Ca_5(PO_4)_3OH$) 10% water solution. The PMMA phantom has a cylindrical shape with a diameter of 27mm with four cylindrical holes, each one with a diameter of 4mm. The acquisition time is 1 second/frame with a tube potential of 100kVp, 500μ A and 1.89mm Aluminum filter. Detector: Medipix3 CdTe-1mm detector. Detector mode: fine pitch mode - charge summing mode (FPM-CSM)

2.1 Imaging System

We used a polychromatic microfocus x-ray tube (Hamamatsu L8121-03) with an adjustable tube peak voltage (40 - 150 kV) and current (0 - 500 μ A). The tube potential was kept constant at 100 kV with a current of 500 μ A. We operated the x-ray source using a focal spot size of 70 μ m. The source to object and the object to detector distances remained similar for all data sets, in the range of 60-65 cm and 9-10 cm, respectively. We gathered the data using a 55 μ m bump bonded CdTe WidePix detector (tiled version of 5 Medipix3RX single-chip units) used in FPM-CSM (fine pitch mode - charge summing mode). The detector was first energy-calibrated using our previously proposed methods.¹³ The WidePix detector has a 1000 μ m CdTe sensor screening an active area of 1.408cm × 7.040cm. For all these multi-material phantom measurements, 290 projections were acquired over a 290-degree arc.

2.2 Materials

To illustrate the separation of contrast agent and bone, we prepared a four-material phantom containing water, Poly-methyl methacrylate (PMMA), hydroxyapatite($Ca_5(PO_4)_3OH$), potassium iodide(KI) and Gadopentetic acid ($C_{14}H_{20}GdN_3O_{10}-H_2O$), see Fig 1. These are common materials that have been used in various other material decomposition studies¹⁴ and are relevant to medical imaging. PMMA is a commonly used tissue surrogate with attenuation properties similar to soft tissue. Hydroxyapatite is a relatively high calcium content material and is the primary constituent of bone and calcifications. Iodine and Gadolinium are the active elements used in approved contrast agents to highlight regions of interest in the human body because their characteristic K-edge lies in the range of typical medical imaging energies.

2.3 Theory

2.3.1 Signal-to-thickness calibration(STC)

PCDs is a promising technology, but still has several deficiencies; some common detector issues are charge sharing, pulse pileup effects, partial charge collection, inter-pixel response variability, and fluorescence photons released by the detector's material. 7,15,16 Without correction, the measured attenuation coefficients are underestimated, 17 and reconstruction artefacts plague the obtained CT image. To correct for inter-pixel variability, we implemented signal-to-thickness calibration (STC) similar to the one done by Jackubeck et al. 18 which we have adapted to CT reconstruction. For the STC, we used fifteen different thicknesses of polymethyl methacrylate (PMMA). The dependence of the detected count rate on the PMMA thickness is measured (calibrated) for each pixel in the detector. We have chosen to use PMMA as its attenuation properties are similar to those typically found in soft tissue. We fitted the following exponential attenuation model to each energy window E as:

$$I_E(T_E) = A_E e^{B_E T_E} \tag{1}$$

where A_E and B_E are fitting parameters for energy window E, and T_E is the calibration material thickness for that energy window. These parameters $\{A_E, B_E\}$ are obtained for each pixel independently. Subsequently, the measured count rate I_E is transformed into equivalent PMMA thickness δ_E^{PMMA} .

After signal-to-thickness calibration, we performed CT reconstruction using 230 projection images for five different energy windows. A slice of the CT reconstruction of the phantom is shown in Fig 1. Because of the energy resolving capabilities of our WidePix (CdTe-1mm) detector, we get five 3D images, one for each one of the five energy windows used in this measurement: 20-26, 26-32, 32-42, 42-50, and 50-60keV.

2.3.2 Mass attenuation correction

To restore the measured mass attenuation values, we associate the measured voxel size of our CT reconstruction with the measured equivalent PMMA thickness values δ_E^{PMMA} using the following relation:

$$\Delta \quad \mu_E = \delta_E^{PMMA} \quad \mu_E^{PMMA} \tag{2}$$

The above equation relates the mass linear attenuation μ_E of an unknown material for energy window E to the equivalent PMMA thickness δ_E^{PMMA} for the same energy window E. Δ is the voxel size in our CT reconstruction (mm), and μ_E^{PMMA} is the theoretical mass attenuation of PMMA (obtained from the NIST database). From this, we get to the corrected linear mass attenuation coefficients μ_E of an unknown material for energy window E.

To test our correction technique, we compared the measured mass attenuation values of several known materials with the expected NIST values, see Fig 2. The corrected mass attenuation agrees with the expected theoretical values for most energies; however, it fails to capture the K-edge effects. At the K-edge energy of iodine, there is a mismatch between experimental results and NIST values attributed to charge sharing effects, which our signal-to-thickness calibration does not remove.

2.3.3 Data clustering using unsupervised clustering

Due to the high amount of spectral information generated by PCDs, cluster analysis or other sophisticated statistical methods are needed to make the most of the data. Our work applies unsupervised machine learning (Gaussian Mixture Model) iteratively to cluster each voxel using mass attenuation values. Unsupervised learning methods such as Gaussian Mixture Model (GMM) allow for different ellipsoidal shapes, sizes, densities and orientations. GMM has advantages over other popular clustering algorithms such as K-means, which fail when the clusters have varying sizes, densities, or non-spherical shapes. We organize voxels into clusters with similar mass attenuation properties. The result of this iterative clustering process is that each voxel in the sample is classified as belonging to one "fundamental" clusters, containing one or more constituent materials in a mixture (e.g. 1-3 materials). In other words, we solve the decomposition problem through a series of steps, each time using cluster analysis to separate one new material from the multi-material object. After clustering, each voxel in the volume has only a limited number of material basis to solve. Finally, we use least-squares to determine the concentration of the reduced set of possible materials.

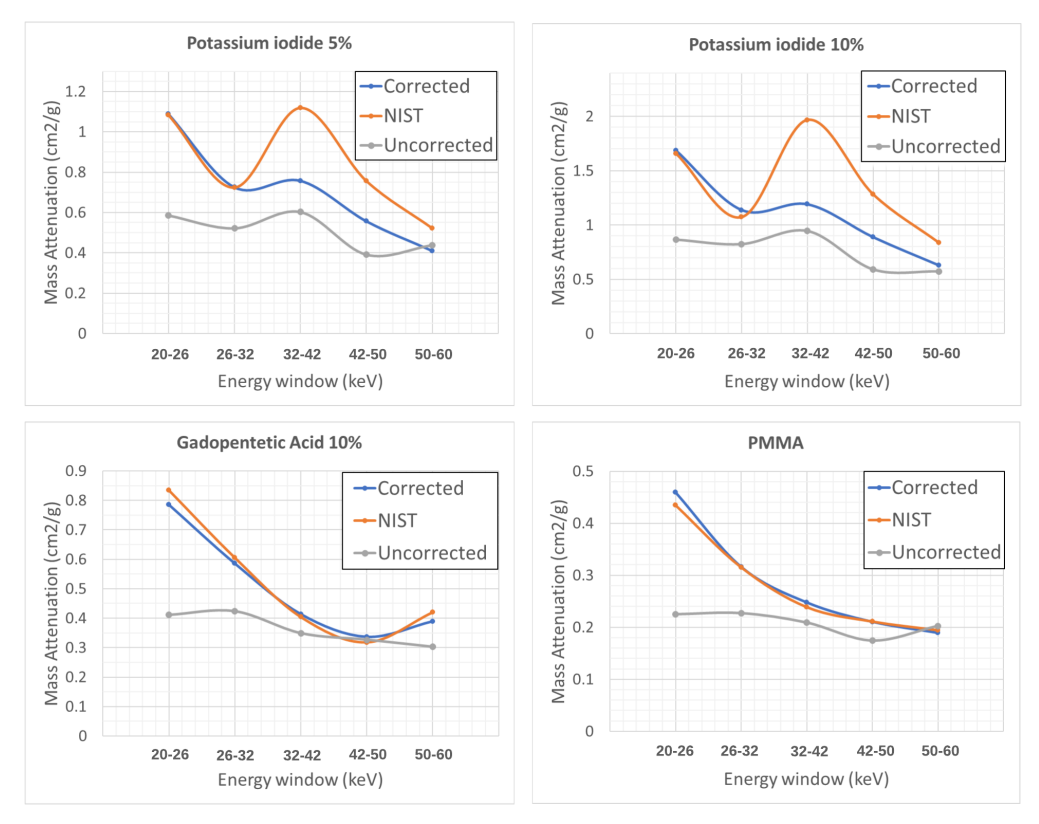


Figure 2: This graph makes a comparison of corrected and uncorrected mass attenuation against expected values obtained from the National Institute of Standards and Technology (NIST) database. There is a good agreement between measured and expected mass attenuation values except for the K-edge effects of iodine, which is not fully captured by our correction. The difference between the theoretical and corrected values is attributed to charge sharing effects which degrade spectral resolution. Tube potential 100 kVp, current $500 \mu\text{A}$ and 1.89 mm Aluminum filter. Detector: Medipix3 CdTe-1mm detector. Detector mode: fine pitch mode - charge summing mode (FPM-CSM)

3. RESULTS

3.1 The benefits of spectral correction on voxel clustering

From data acquisition to material decomposition, there are several data processing steps. First, we collect multienergy computed tomography measurements using a CdTe-1mm Medipix detector. This step gives us a set of projections for each energy window. Subsequently, using signal-to thickness calibration, these projections are converted to equivalent PMMA thickness using Eq??. The PMMA equivalent projections are then reconstructed to obtain 3D multi-energy images of the object. Subsequently, the equivalent PMMA thickness of each voxel is converted into mass attenuation values using Eq??. Then, we apply cluster analysis in steps, separating one new material at a time from the multi-material object. We classify the most abundant materials first, usually air and soft tissue. Then we proceed with the materials that have more similar mass attenuation values, each time "zooming" into materials with more similar mass attenuation. We repeat this process until we reach the "fundamental" cluster, for which no further cluster differentiation is possible. Finally, we obtain the maps of each material within the object using a least-squares material decomposition. A general overview of the different steps involved in the data processing pipeline is illustrated in Fig 3.

To test the effect of spectral correction on voxel clustering, we compare the results obtained after cluster analysis. Fig 4 shows the fundamental clusters obtained for two different experimental conditions. In the first

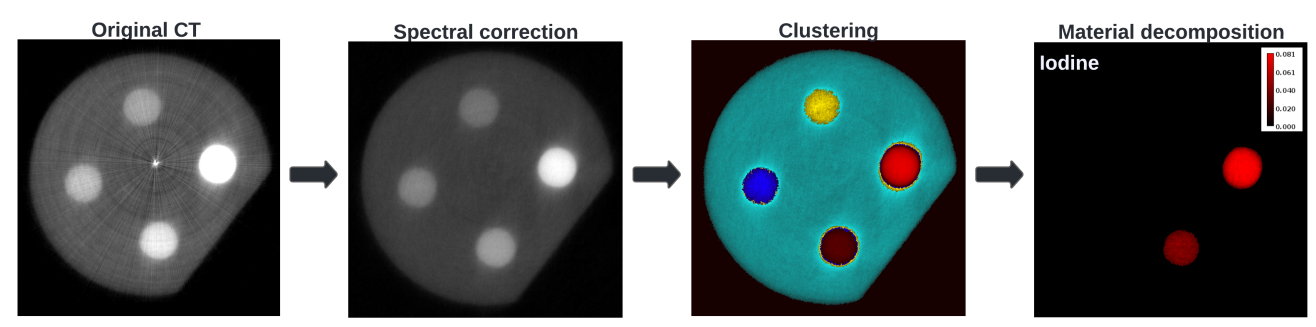


Figure 3: This figure shows an overview of the main steps in the data processing pipeline: spectral correction, cluster analysis, and material decomposition. Our spectral correction reduces voxel misclassification at the boundaries between materials by reducing noise and removing beam hardening effects. The several clusters are: PMMA (cvan), potassium iodide(red), Gadopentetic acid(vellow), and Hydroxyapatite(blue).

situation Fig $4(\mathbf{A})$, we applied only a flat-field correction to the projection images. Beam hardening effects generate much of the noise present in the reconstruction, especially towards the centre of the PMMA phantom. The pixel-to-pixel variability also increases voxel misclassification, which leads to noise and rings of incorrectly classified voxels.

In the second situation, see Fig $4(\mathbf{B})$ we have the results of using our spectral correction. In both situations, we used all five energy windows (20-26, 26-32, 32-42, 42-50 and 50-60keV) for classification. We observed a significant noise reduction in this situation, and many voxels that were initially misclassified using dual-energy are now successfully classified when using more than two energy windows. However, we still have incorrectly classified voxels at the boundary between materials, suggesting that mass attenuation values alone are insufficient for complete tissue classification in a complex mixture of materials.

3.2 Material decomposition using multi-contrast agents

The mass attenuation can be written as a linear combination of all the materials present in that voxel.^{9–11} After the clustering step, we use least-squares to determine mass fractions, each cluster having only a limited number of material basis to solve.

Fig. 2 shows how the corrected mass attenuation values deviate from the theoretical NIST values for the energy window 32-42keV, which prevents us from using this energy window for material decomposition. This is why after voxel classification, we only use 20-26 and 26-32 keV for material decomposition, avoiding using the iodine K-edge energy range because our spectral correction does not fully capture the K-edge effects.

$$\mu_M(E) = \sum_{i=1}^{N} m_i \, \mu_{M,i}(E), \text{ subject to}$$

$$\sum_{i=1}^{N} \beta_i = 1, \quad 0 \le \beta_i, \quad i = 1, ..., N$$
(3)

where $\beta_i = \frac{m_i}{\sum_{i=1}^N m_i}$ is the mass fraction of each constituent material and m_i is the total mass of material i in the mixture.

After cluster analysis, each cluster has a tailored set of values $\{\mu_{M,i}\}$ that correspond to the reduced set of the possible material basis. These mass attenuation values used for material decomposition are obtained from the National Institute of Standards and Technology (NIST) database.

We tested our iterative clustering decomposition method using a phantom, see Fig 1. The benefits that spectral correction brings to material decomposition quantification could be seen in reduced errors in classifications. The measured mass fractions agreed with nominal values, with a maximum error of 3.75% for Iodine and 9.3% for Gd. Spectral correction plays a fundamental role in the accuracy of measured mass fractions. Due to the detector defects, the measured mass attenuation values are meaningless without spectral correction.

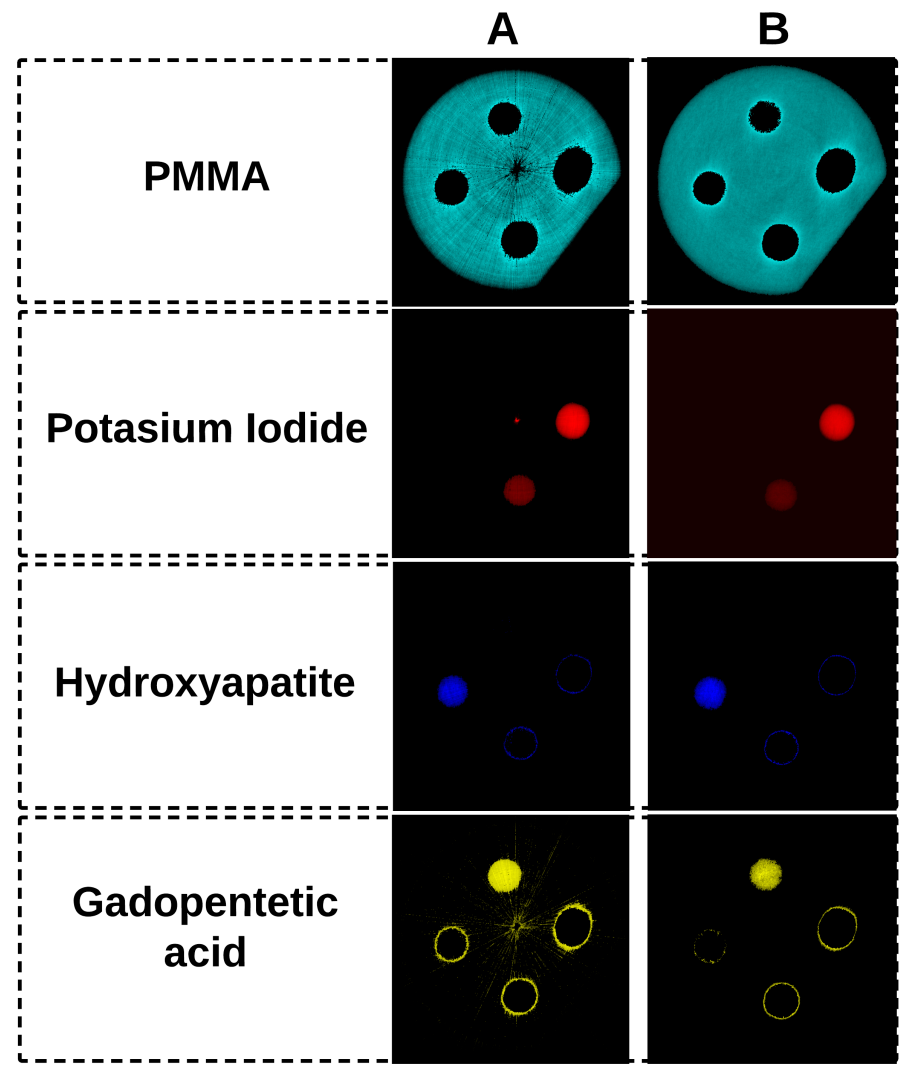


Figure 4: Fundamental clusters obtained for different conditions. **A**) Only flat-field correction was applied to the projection images. **B**) Using our spectral correction. On both situation we used five energy windows for voxel classification: 20-26, 26-32, 32-42, 42-50, and 50-60keV. The acquisition time is 1 second/frame with a tube potential of 100kVp, $500\mu\text{A}$ and 1.89mm Aluminum filter. Detector: Medipix3 CdTe-1mm detector. Detector mode: fine pitch mode - charge summing mode (FPM-CSM).

4. CONCLUSIONS AND DISCUSSION

Material decomposition of tissues and organs is challenging because most material decomposition methods can only deal with two material basis. Nevertheless, several methods have been proposed to bypass the two-material limitation of dual-energy CT. Many of these methods rely on the spectroscopic capabilities of photon-counting detectors and the K-edge effect to reduce the number of material basis to solve. However, the performance of all these decomposition methods depends on the accuracies of the measured attenuation values, which can be heavily affected by detector distortions. We implemented a signal-to-thickness calibration to eliminate inter-pixel variability and restore the measured mass attenuation to theoretical NIST values. We have presented experimental proof showing how our spectral correction significantly reduces material decomposition error and noise compared to flat-field correction. One of the main advantages of our approach is its simplicity and versatility, as it does not require the formulation of a model for our PCD. However, our correction does not fully recover the

photons lost in charge sharing events, which improvements to the PCD's hardware can only solve.

This work has demonstrated the benefits of using spectral correction and unsupervised clustering on material decomposition. We iteratively used a Gaussian Mixture Model to group voxels according to similar attenuation properties. We consistently obtained better clustering results when using more than two energy windows; the voxels originally misclassified using dual-energy were correctly classified when using more energy windows. Furthermore, by utilizing all the spectral information, we take advantage of the unique K-edge effects of iodine and gadolinium. Moreover, we also show that material segmentation based on attenuation values alone may not be enough. When using only corrected mass attenuation values for clustering, the segmentation fails at the boundaries between different materials. One possible solution to this may be to incorporate spatial information during classification. It may be necessary to include texture features during clustering to reduce noise and miss-classification at the edges between different materials. Reducing the misclassification at the edges between different materials could improve the delineation of gross target volumes in radiotherapy. There could also be benefits in including spectral scatter signatures as they have shown to improve estimation accuracy in x-ray imaging with photon counting detectors.¹⁹

When combining our spectral correction with unsupervised iterative clustering, we can better use the spectral information that PCDs provide, which allows for the reliable separation of contrast agents and multi-material decomposition.

5. ACKNOWLEDGEMENTS

This work was partially supported by funding from the NIH National Institute of Biomedical Imaging and Bioengineering (NIBIB) grant R01 EB EB029761, US Department of Defense (DOD) Congressionally Directed Medical Research Program (CDMRP) Breakthrough Award BC151607 and the National Science Foundation CAREER Award 1652892.

REFERENCES

- 1. M. Firsching, A. P. Butler, N. Scott, N. G. Anderson, T. Michel, and G. Anton, "Contrast agent recognition in small animal CT using the Medipix2 detector," **607**(1), pp. 179–182.
- C. J. Bateman, J. McMahon, A. Malpas, N. De Ruiter, S. Bell, A. P. Butler, P. H. Butler, and P. F. Renaud, "Segmentation enhances material analysis in multi-energy ct: A simulation study," in 2013 28th International Conference on Image and Vision Computing New Zealand (IVCNZ 2013), pp. 190–195, IEEE, 2013.
- 3. S. Tao, K. Rajendran, C. H. McCollough, and S. Leng, "Feasibility of multi-contrast imaging on dual-source photon counting detector (pcd) ct: An initial phantom study," *Medical physics* **46**(9), pp. 4105–4115, 2019.
- R. Symons, B. Krauss, P. Sahbaee, T. E. Cork, M. N. Lakshmanan, D. A. Bluemke, and A. Pourmorteza, "Photon-counting ct for simultaneous imaging of multiple contrast agents in the abdomen: an in vivo study," Medical physics 44(10), pp. 5120–5127, 2017.
- 5. N. R. Fredette, A. Kavuri, and M. Das, "Multi-step material decomposition for spectral computed tomography," *Physics in Medicine & Biology* **64**(14), p. 145001, 2019.
- 6. L. Ren, B. Zheng, and H. Liu, "Tutorial on x-ray photon counting detector characterization," *Journal of X-ray science and technology* **26**(1), pp. 1–28, 2018.
- K. Taguchi and J. S. Iwanczyk, "Vision 20/20: Single photon counting x-ray detectors in medical imaging," Medical physics 40(10), p. 100901, 2013.
- 8. J. Jakubek, "Data processing and image reconstruction methods for pixel detectors," Nuclear Instruments and Methods in Physics Research Section A: Accelerators, Spectrometers, Detectors and Associated Equipment 576(1), pp. 223–234, 2007.
- 9. H. Q. Le and S. Molloi, "Least squares parameter estimation methods for material decomposition with energy discriminating detectors," *Medical physics* **38**(1), pp. 245–255, 2011.
- 10. S. Lee, Y.-N. Choi, and H.-J. Kim, "Quantitative material decomposition using spectral computed tomography with an energy-resolved photon-counting detector," *Physics in Medicine & Biology* **59**(18), p. 5457, 2014.

- 11. H. Q. Le and S. Molloi, "Segmentation and quantification of materials with energy discriminating computed tomography: A phantom study," *Medical physics* **38**(1), pp. 228–237, 2011.
- 12. A. M. Alessio and L. R. MacDonald, "Quantitative material characterization from multi-energy photon counting ct," *Medical physics* **40**(3), p. 031108, 2013.
- 13. S. Vespucci, C. S. Park, R. Torrico, and M. Das, "Robust energy calibration technique for photon counting spectral detectors," *IEEE Transactions on Medical Imaging* **38**(4), pp. 968–978, 2019.
- 14. N. R. Fredette, A. Kavuri, and M. Das, "Multi-step material decomposition for spectral computed tomography," **64**(14), p. 145001.
- 15. K. Taguchi, K. Stierstorfer, C. Polster, O. Lee, and S. Kappler, "Spatio-energetic cross-talk in photon counting detectors: Numerical detector model (pc tk) and workflow for ct image quality assessment," *Medical physics* 45(5), pp. 1985–1998, 2018.
- 16. S. S. Hsieh, P. L. Rajbhandary, and N. J. Pelc, "Spectral resolution and high-flux capability tradeoffs in cdte detectors for clinical ct," *Medical physics* **45**(4), pp. 1433–1443, 2018.
- 17. T. G. Schmidt, "Ct energy weighting in the presence of scatter and limited energy resolution," *Medical physics* **37**(3), pp. 1056–1067, 2010.
- 18. J. Jakubek, "Data processing and image reconstruction methods for pixel detectors," 576(1), pp. 223–234.
- 19. C. E. Lewis and M. Das, "Spectral signatures of x-ray scatter using energy-resolving photon-counting detectors," Sensors 19(22), 2019.